Journal Applied Mechanics and Technical Physics, Vol. 36, No. 4, 1995

APPLICATION OF A CHARGE-EXCHANGE PROCESS TO OPTICAL DIAGNOSTICS OF THE INTERACTION OF A LASER-GENERATED PLASMA WITH A DIPOLE MAGNETIC FIELD

I. F. Shaikhislamov, V. M. Antonov, Yu. P. Zakharov, A. V. Melekhov, V. G. Posukh, and V. O. Stoyanovskii

UDC 621.378.826:533.9

The paper presents the results of applying a charge-exchange process in recording ion concentrations in model experiments with a laser-generated plasma. A new diagnostic method has been employed in an experiment on laser-generated plasma expansion in a dipole magnetic field. New quantitative as well as qualitative data on plasma dynamics, which may be of interest in studying explosive processes in the earth's magnetosphere [1, 2], are obtained. The present paper is devoted for the most part to application of the new diagnostics.

1. A Method for Determining Plasma Ion Density from the Emission Induced by Charge Exchange. Let us consider a free-expanding plasma cloud generated by laser irradiation of a target. The line emission of such a plasma expanding into a vacuum is of a purely recombination nature. When a background gas is allowed to bleed in (on the condition that the path of elastic collisions between the plasma and the gas is much greater than the size of the observation area), the charge-exchange reaction causes the emission attributed to the charge-exchange ion excitation:

$$C^{i+1} + H_2 \to C^i_{exc} + H_2^+ \to C^i + H_2^+ + \gamma.$$

Here i is the ion charge; H_2 (molecular hydrogen) is the background gas used in the experiments; γ is a light quantum.

It is well known that the emission of certain lines by an ion of charge i is most sensitive to charge exchange at relatively low collision energies. The emission of such lines as a function of gas concentration was investigated in [3]. Equations describing the charge-exchange interaction and the emission from a laser-generated plasma with a background gas are analyzed in [4].

Let the following conditions be fulfilled:

$$n_{i+1} \gg n_{i+2} \quad (n_i \text{ is the concentration of ions of charge } i \text{ in the plasma}), \quad R_c \ll R_\sigma^{i+1},$$

where $R_c = \sqrt{\sum_i N_i \sigma_i}$; N_i is the total number of ions of charge i that passed through an observation point in a unit solid angle; σ_i is the cross section of charge exchange of an ion of charge i into $i-1$; $R_\sigma^i = 1/n_b/\sigma_i$ is the path of charge exchange of an ion of charge i with background gas of concentration n_b. Then the ion emission J_i that is induced by the charge exchange is related to the concentration n_{i+1} of the ion $i+1$ in the following way:

$$n_{i+1}(R,t) \sim J_i(R,t) \exp\left[(R_c/R)^2 + R/R_\sigma^{i+1}\right]/\sigma_{i+1} V$$

(R is the distance from the observation point to the target; V is the ion velocity).

It can be seen that the method is applicable in the range $R_c < R < R_\sigma$. When $R < R_c$, there are no neutrals because they are completely charged by the plasma cloud at these distances, while for $R > R_\sigma$

Institute of Theoretical and Applied Mechanics, Novosibirsk 630090. Translated from Prikladnaya Mekhanika i Tekhnicheskaya Fizika, Vol. 36, No. 4, pp. 8–15, July–August, 1995. Original article submitted June 6, 1994; revision submitted July 29, 1994.

 0021-8944/95/3604-0488 $12.50

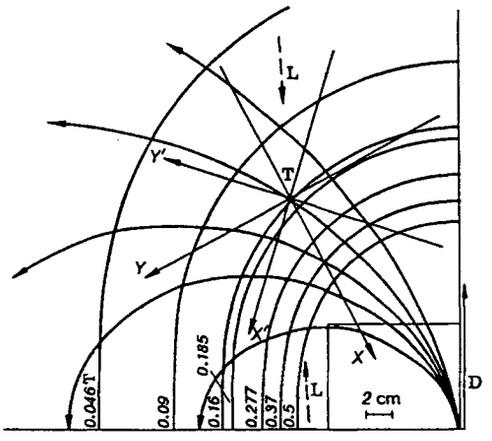

Fig. 1

the number of ions in the cloud decreases sharply due to charge exchange with the neutrals. The method is implemented practically in the following way. An experimental volume is filled with a neutral gas, and a corresponding emission line of an appropriate plasma ion is selected in such a way as to satisfy all conditions listed above and to excite sufficiently intense charge-exchange emission. In so doing, one should discern this charge-exchange emission against the background of the recombination emission existing primordially. For $R \ll R_\sigma$ a change in the ion composition is insignificant, and, as was established in [5], variations in the temperature of the laser-generated plasma are also insignifcant at gas pressures $p < 10$ Pa and a plasma concentration greater than or of the order of the gas concentration. By this is meant that, on letting the gas in, the charge-exchange emission is added to the invariable recombination one. Therefore, to select the necessary emission of an ion line, one should measure the emission of this line with and without the gas and then subtract one from the other.

2. Experimental Procedure. Except for the dipole magnetic field, the experimental procedure is similar to that given in [4]. Experiments with a dipole magnetic field were first described in detail in [1].

The experiments were carried out on a KI-1 bench in a chamber 1.2 m in diameter and 5 m in length [6]. A CO_2 amplifier, which generated a bell-shaped pulse 100 nsec wide at half-height points, produced a plasma cloud. A caprolon ($C_6H_{11}ON$) spherical pellet 4 mm in diameter was used as a target. A quasispherical plasma cloud with total number of ions $N_0 = 2.5 \cdot 10^{17}$, front expansion velocity $V = 2 \cdot 10^7$ cm/sec, and total energy $E_0 = 7$–10 J was produced by irradiating the pellet from two opposite directions with laser beams focused to spots with a diameter of 7 mm. At the laser radiation intensities used ($\sim 10^{10}$ W/cm^2), the front part of the cloud is largely composed of hydrogen and carbon ions of charge +3 and +4.

To detect the emission from the plasma, we applied an image converter tube (ICT) operating in the frame regime with an exposure duration of 50 nsec and a spatial resolution of 0.5 cm. An interference filter selected the required spectral interval [4].

The plasma emission was detected with the use of a filter ($\Delta\lambda = 5$ nm) for the doublet line 580.1 and 581.1 nm of the C^{+3} ion. This visible line is most excited when the C^{+4} ion exchanges charges with H_2 [3] with the charge-exchange cross section $\sigma = 2 \cdot 10^{-15}$ cm^2 [7]. The residual gas pressure in the chamber was $p = 5 \cdot 10^{-4}$ Pa. To induce the charge exchange, hydrogen H_2 was let in up to a pressure of $p \leqslant 0.05$ Pa. It follows from the experiment parameters that $R_c = \sqrt{N_0 \sigma / 4\pi} = 4$ cm, $R_\sigma = 1/n_b\sigma > 20$ cm, i.e., the condition $R_c \ll R_\sigma$ was fulfilled to a sufficient degree.

The plasma concentration was measured with electrical cylindrical Langmuir probes 15 μm in diameter which consisted of three mutually orthogonal electrodes with an equal length (7–8 mm). Magnetic field perturbation structures were measured with broad-band three-component magnetic probes which were shielded by a slotted foil and isolated from the plasma by a glass tube with $\phi = 5$ mm.

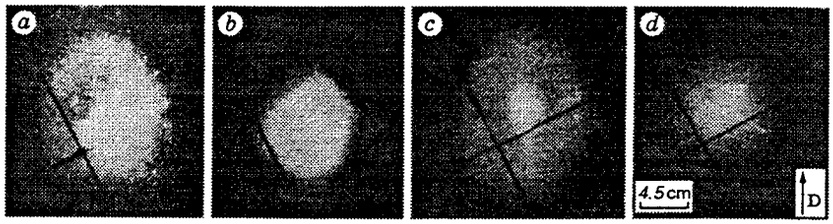

Fig. 2

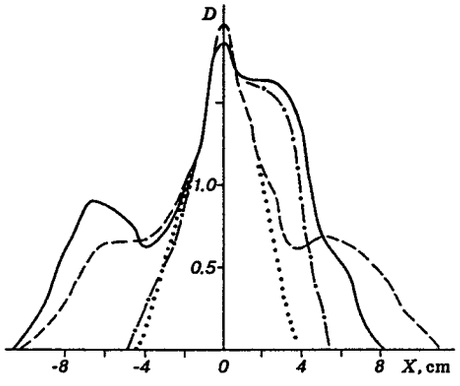

Fig. 3

Figure 1 shows the experiment geometry: the position of the dipole moment D, the lines of force and level of the absolute value of magnetic field, the locations of the target T and the coordinate system which are used below, and the incidence directions of two laser beams L. The ICT plane of image recording coincides with the figure plane. The dipole magnetic moment was 10^3 T·cm^3.

3. Experimental Results. *Analysis of the method.* The present paper describes in detail the results of photographing the plasma at time $t = 0.55$ μsec from the beginning of plasma formation. This precisely the instant of time when the experimental conditions make it possible to distinguish most clearly the characteristics of the method in question. In addition, the results of interaction of the expanding plasma cloud with the dipole magnetic field begin to manifest themselves by this time, which allows us to draw definitive conclusions about the interaction dynamics.

Figure 2 presents four photographs of the emission from the plasma, which were taken with a filter for the C^{+3} ion line [(a) corresponds to $B_0 \neq 0, p = 0.05$ Pa; (b) to $B_0 \neq 0, p = 0$; (c) to $B_0 = 0$ $p = 0.05$ Pa, (d) to $B_0 = 0, p = 0$].

Figure 3 shows the density D of the photographs in Fig. 2a–d along the X axis: the solid line corresponds to Fig. 2a (with the gas, in the magnetic field); the dot-dash line corresponds to Fig. 2b (without gas, in the magnetic field); the dashed line corresponds to Fig. 2c (with the gas, in the absence of magnetic field); the doted one to Fig. 2d (in the absence of gas and magnetic field). It can be seen that the recombination emission (the emission without gas) remains predominant and virtually unchanged within < 3 cm of the target. In the magnetic field at a distance of 4 cm, the emission in the presence of gas is greater than the emission in the absence of gas by at least 2.5 times, while at long distances it becomes obviously predominant. As was noted above, the intrinsic charge-exchange emission can be obtained simply by subtracting the emission in the absence of gas from the emission in the presence of gas.

Figure 4 shows results of subtraction in the magnetic field (solid line) and without it (dashed) in eight directions from the target. The experimental error of such a procedure (besides theoretical assumptions) depends on plasma reproducibility from start to start, ICT stability, and photofilm quality and, in this case,

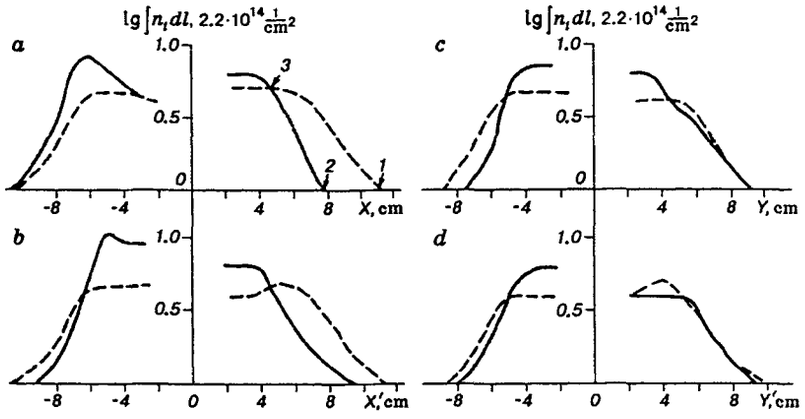

Fig. 4

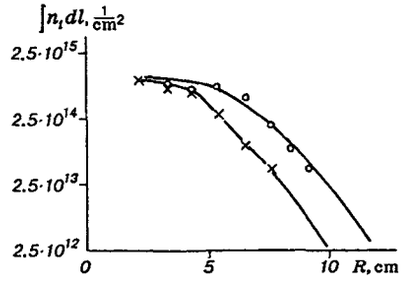

Fig. 5

can run to 30%. Since a photograph collects the emission integrated over a line of sight, the quantity $\log \int n_i\, dl$ (below n will denote just ion concentration) is plotted in Fig. 4 rather than the density D caused by the charge-exchange emission. Figure 4 provides original experimental data.

To verify the results obtained in such a manner, we made a comparison with the data obtained in the probe measurements. Figure 5 shows density D curves for the plasma emission photograph taken at time $t = 0.45$ μsec on the C^{+3}-ion line at an H_2 pressure in the chamber of 0.02 Pa; the circles correspond to the points of the photometric curve in the X direction, while the crosses correspond to those in the Y direction; the lines are the charge-averaged ion concentration profiles integrated over the ICT line of sight and obtained in probe measurements in the same directions. The integral over the line of sight of the probe measurements was calculated under the assumption of spherical symmetry of the cloud. Since the optical method in question is relative, the absolute calibration of an optical signal was chosen from the condition of the best agreement with the probe measurements.

It can be seen that the profiles agree quite satisfactorily. The maximum deviation at an individual point is 40%, while the average one is 15%. It should be noted that the dynamic range of optical measurements is considerably less than that of probe measurements (as is seen from Fig. 5). This is related to the smaller range of the photofilm and the presence in the plasma of a hydrogen forerunner which is measured by the probes but is not detected by the optical method employed. Nevertheless, according to Fig. 5, the optical measurements cover respectively over 75% and 90% of the corresponding cloud energy and the number of particles in the cloud that were obtained in the probe measurements.

The results from a comparison of (Fig. 4) the apparent front velocity with the probe measurement data show that they also cover no less than 90% of cloud particles and 75% of its energy. Hereafter the absolute calibration of an optical signal will be carried out against the total number of ions in the cloud, which was measured by the probes. According to the probe measurements, the mean number of ions in the

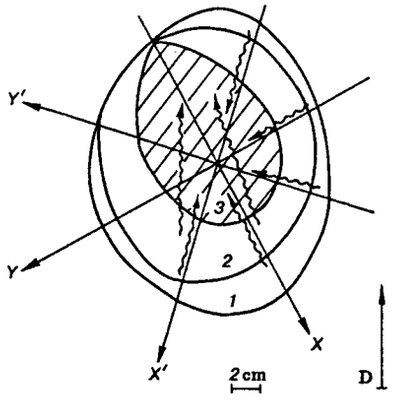

Fig. 6

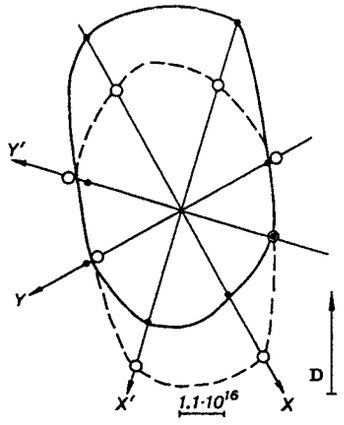

Fig. 7

cloud $\langle N_0 \rangle = 2.5 \cdot 10^{17}$; their mean charge $\langle Z \rangle = 2.5$ and mean mass $\langle M \rangle = 6.6$ amu. Practically, this integral calibration does not differ from the one presented in Fig. 5 but is of a more general nature if a plasma cloud is considered as a whole without regard to its ion composition. Thus, for the calibration factor A we have

$$A \iint n \, dl \, dS = \langle N_0 \rangle,$$

where $\int dS$ is taken over the whole photographing plane.

Plasma interaction with a dipole magnetic field. According to the model suggested, Fig. 4 presents the profiles of the relative quantities n integrated over the line of sight. From this point on, we shall restrict our consideration to the integral quantities $\int n \, dl$ without resorting to calculation of n because in this case the physical experimental conditions are symmetric with respect to the observation plane, and plasma dynamics is most interesting precisely in the observation plane (see Fig. 1).

Comparison of the charge-exchange emission in the presence and absence of the dipole field at time $t = 0.55$ μsec clearly shows deceleration of particles at the plasma front and their movement. Three characteristic sizes can be pointed out: points *1* and *2* in Fig. 4a (the visible emission front in the absence and presence of the magnetic field), and point *3* after which the emission in the field exceeds the emission in its absence. In Fig. 6, these areas, constructed in eight directions from the target, are presented in the whole observation plane.

Figure 7 presents hodographs of the total number of particles in eight directions from the target: $(2\pi/8) \int r \, dr \int n \, dl$; the open circles correspond to the case of absence of the dipole field; the filled to ones, its presence.

Comparison of Figs. 6 and 7 shows that the relative movement of particles occurs in much the same manner as the arrows show in Fig. 6. The transference of the particles from the X and X' directions to the $-X$ and $-X'$ directions, apart from their usual radial deceleration, is a relatively new effect. The decrease in the number of particles in the area between curves *1* and *3* is 20% of their total number in the cloud, while the number of the particles that experience a considerable transference from the X and X' directions to $-X$ and $-X'$ runs to 12% respectively.

The effect of the significant transference of the particles and the increase in their total number in some directions seems rather unusual. However, the probe measurements performed along the $-X$ axis reveal the same effect, namely: according to the probe measurements the total number of particles in a unit solid angle along the $-X$ axis increases 1.5 times at $t = 0.55$ μsec on switching on the dipole field. This is in good agreement with the optical data (Fig. 7).

Figure 8 shows hodographs of radial plasma energy in the observation plane in eight directions from the target:

$$(\langle M \rangle/2)(2\pi/8) \int (r/t)^2 \, r \, dr \int n \, dl$$

TABLE 1

Direction	R_{pl}/R_b	$\Delta E/E_0, \%$	L_b	L_n
			cm	
X	2	75	1.85	1.8
X'	2.5	45	1.0	2.0
Y	1.4	0	3.0	2.7
Y'	0.74	0	2.85	2.3
$-X$	1.1	0	2.4	2.2
$-X'$	1.4	35	0.6	1.1
$-Y$	1.9	40	1.0	1.1
$-Y'$	1.4	40	1.4	1.5

(open circles correspond to the case of no field; filled circles to the presence of field). The energy in the magnetic field was calculated without regard for the transferred particles, i.e., the particles that increased the plasma concentration in the area up to curve *3* in Fig. 6. The total radial energy of the plasma decreased from 8.4 J with no field to 5.5 J in the dipole field, i.e., the plasma lost 36% of the kinetic energy of radial motion in the interaction with the dipole field.

It should be noted that in the general case this method gives no way of drawing a conclusion about the part of the plasma energy that is related to the motion along the line of sight.

Optical data are compared with measurements of the magnetic field perturbation ΔB at $t = 0.55$ μsec in Fig. 9. Curves *1*–*3* correspond to the levels of field decrease by 0.01, 0.04, and 0.1 T.

The data comparison shows that the assumed boundary of magnetic field perturbation of 0.01 T (which is at most 20% of the minimum dipole field) coincides with the plasma emission boundary (the dashed line) where the deceleration is not observed. From this follows the conclusion that the observed magnetic field perturbation is attributed to the plasma part that is entirely within the sensitivity range of optical measurements. At the same time, the inherent emission of the plasma without gas (Fig. 2b) is localized within the perturbation boundary $\Delta B = 0.04$ T.

It is interesting to note that the relative gradients of the field perturbation and of the concentration turn out to be close to each other:

$$1/L_n \equiv |\nabla n|/n \approx 1/L_b \equiv |\nabla \Delta B|/\Delta B.$$

Experimentally measured values of L_n and L_b are presented in Table 1 for comparison. To calculate L_n, a measured value of $\int n\, dl$ was taken. This is justified because the characteristic variation scale is not more than 2 cm, while the characteristic path L_n is not less than 6 cm; therefore the error is $L_n/2l = 15\%$.

As is seen from Table 1, L_n and L_b are in good agreement for six directions. Only for the X' and $-X'$ directions, where ΔB is an anomalously high local gradient (see Fig. 9), is L_b two times less.

4. Comparison with a Theoretical Model. The interaction of plasma flows with an inhomogeneous magnetic field is a complex problem, and at present there are no approved analytical models. A magnetohydrodynamic model for plasma cloud deceleration in a dipole magnetic field was suggested in [1]. Using this model, one can calculate the plasma deceleration boundary R_b with regard for the initial distribution of kinetic energy $dE_0/d\Omega(f)$ in the cloud, where the angle f is reckoned in the observation plane. Since, under certain assumptions, the initial distribution $dE_0/d\Omega(f)$ can be restored from the radial plasma energy measured integrally over the line of sight, the plasma energy loss $\Delta E/E_0$ as a function of R_{pl}/R_b can be constructed in eight directions from the target. Here R_{pl} is the visible boundary reached by the plasma (curve *2* in Fig. 6), while R_b is calculated according to [1]. As is seen from Table 1, for $R_{pl}/R_b > 1$ the plasma is decelerated, while for $R_{pl}/R_b \leqslant 1$ it is not, which, on the whole, agrees with the model. An obvious deviation from the calculations in the Y direction is also observed. Most probably this is attributed to the fact that the plasma moving in the X direction "presses" the field lines to the dipole (see Fig. 1) with the result that the flow along the X' axis spreads relatively far beyond R_b, while it is not decelerated at all along the Y axis.

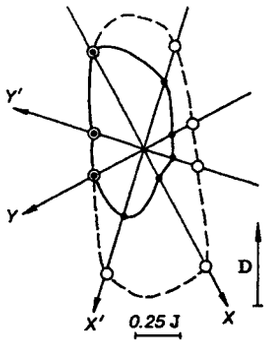

Fig. 8

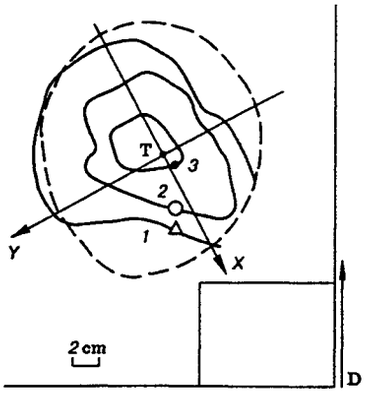

Fig. 9

As Fig. 9 shows, by the time $t = 0.55$ μsec the field penetrated the plasma to a large extent; therefore $\Delta B/B_0 \ll 1$. Under these conditions, the thickness of the plasma current layer is no longer determined by the plasma skin layer. At this stage the magnetic field pressure should be counterbalanced by the pressure of the plasma with ion energy W, including the energy of ordered motion $\langle M \rangle V^2/2$ and of random motion with effective temperature T:

$$4\pi W \nabla n = B_0 \nabla \Delta B, \qquad W = \langle M \rangle V^2/2 + T.$$

Since the quantities B_0 and W_0 change over the size of the whole plasma cloud ($\sim$ 10 cm), while n changes over a much shorter length ($\sim$ 2 cm), the gradient ΔB must be dictated by the concentration gradient. This is precisely what was detected in the experiment.

Thus, the new optical method for measuring a plasma concentration, which was applied in the experiment on laser-generated plasma interaction with a dipole magnetic field, showed qualitative and quantitative agreement with theoretical estimates as well as with independent magnetic and electric measurements. The results obtained allowed us to reveal essential details of plasma particle motion and to describe quantitatively the character of plasma cloud interaction with an inhomogeneous magnetic field. It has been demonstrated that the inherent plasma emission does not reflect the true distribution of the particles that interact with the magnetic field, and only the application of the new diagnostic method based on charge exchange has made it possible to detect them.

The authors are grateful to A. G. Ponomarenko and A. M. Orishich for useful discussions and to V. N. Snytnikov for his help in performing the experiments.

This work was supported by the Russian Foundation for Fundamental Research (Grant 95-02-04605-a).

REFERENCES

1. S. A. Nikitin and A. G. Ponomarenko, "Dynamics of the spatial boundary of deceleration of a plasma explosion cloud in a dipole magnetic field," *Prikl. Mekh. Tekh. Fiz.*, **34**, No. 6, 3–10 (1993).
2. Yu. P. Zakharov, S. A. Nikitin, A. M. Orishich, and A. G. Ponomarenko, "Laboratory simulation of magnetospheric hazard processes," *Proceedings of Intern. Conf. on Hazards due to Comets and Asteroids*, Tucson (1993), pp. 88–89.
3. A. M. Orishich and I. F. Shaikhislamov, "Spectroscopic diagnostics of a plasma expanding into a background gas and a magnetic field," *Prikl. Mekh. Tekh. Fiz.*, **33**, No. 3, 13–19 (1992).
4. Yu. P. Zakharov, A. M. Orishich, V. N. Sytnikov, and I. F. Shaikhislamov, "Application of a charge exchange process to spectroscopic diagnostics of plasma flows," *Prikl. Mekh. Tekh. Fiz.*, **35**, No. 3, 174–180 (1994).
5. R. H. Dixon and R. C. Elton, "Resonance charge transfer and population inversion following C and C interactions with carbon atoms in a laser-generated plasma," *Phys. Rev. Lett.*, **38**, No. 19, 1072–1075 (1977).

6. L. B. Gevorkyan, A. M. Orishich, A. G. Ponomarenko, et al., "Development of methods for simulating some astrophysical phenomena in laboratory experiments," in: *Physical Gas Dynamics*, No. 6 [in Russian], AN SSSR, Sib. Branch, ITPM, Novosibirsk (1976), pp. 192–196.
7. R. Hoekstra, F. J. de Heer, and R. Morgenstern, "Photons shedding light upon basic charge exchange processes," in: *Atomic Physics of Highly Charged Ions*, Springer-Verlag, Berlin (1991), pp. 81–85.